1-1-1991

# Modulated, Frequency-locked, and Chaotic Cross-waves

William B. Underhill
*University of Arizona*

Seth Lichter
*University of Arizona*

Andrew J. Bernoff
*Harvey Mudd College*

*J. Fluid Mech.* (1991), *vol.* 225, *pp.* 371–394
*Printed in Great Britain*



# Modulated, frequency-locked, and chaotic cross-waves

By WILLIAM B. UNDERHILL[1], SETH LICHTER[1] AND ANDREW J. BERNOFF[2]†

[1]Department of Aerospace and Mechanical Engineering, The University of Arizona, Tucson, AZ 85721, USA

[2]Department of Mathematics, The University of Arizona, Tucson, AZ 85721, USA

(Received 28 June 1989 and in revised form 12 September 1990)

Measurements were made of the wave height of periodic, quasi-periodic, and chaotic parametrically forced cross-waves in a long rectangular channel. In general, three frequencies (and their harmonics) may be observed: the subharmonic frequency and two slow temporal modulations – a one-mode instability associated with streamwise variation and a sloshing motion associated with spanwise variation. Their interaction, as forcing frequency, $f$, and forcing amplitude, $a$, were varied, produced a pattern of Arnold tongues in which two or three frequencies were locked. The overall picture of frequency-locked and -unlocked regions is explained in terms of the Arnold tongues predicted by the circle-map theory describing weakly coupled oscillators. Some of the observed tongues are apparently folded by a subcritical bifurcation, with the tips of the tongues lying on the unstable manifold folded under the observed stable manifold. Near the intersection of the neutral stability curves for two adjacent modes, a standing wave localized on one side of the tank was observed in agreement with the coupled-mode analysis of Ayanle, Bernoff & Lichter (1990). At large cross-wave amplitudes, the spanwise wave structure apparently breaks up, because of modulational instability, into coherent soliton-like structures that propagate in the spanwise direction and are reflected by the sidewalls.

## 1. Introduction

### 1.1. *Related theory and experiments*

There have been several recent investigations of the periodic, quasi-periodic, and chaotic behaviour of waves forced by oscillating a container or the wall of a container. Ciliberto & Gollub (1984, 1985) found that two parametrically excited modes (in a circular geometry) with adjacent regions of instability can exchange energy in a periodic or chaotic fashion. Lichter & Underhill (1987) showed that, for cross-waves near the transition frequency from one mode to an adjacent mode, there is a small frequency interval of chaos. Shemer & Lichter (1987) found a quasi-periodic and chaotic region at large forcing amplitude for cross-waves in a long channel. Funakoshi & Inoue (1987, 1988) identified a strange attractor for resonantly forced surface waves in a cylindrical vessel oscillated horizontally. Gu & Sethna (1987) developed a perturbation analysis for parametrically excited waves in a rectangular tank and identified at least three routes to chaos. They also computed

† Current address: Department of Engineering Sciences and Applied Mathematics, Northwestern University, Evanston, IL 60208, USA.

the basins of attraction (Gu, Sethna & Narain 1988) for regions of parameter space in which there are multiple solutions. The dependence of amplitude on detuning at a supercritical bifurcation showed good agreement with experiment (Virnig, Berman & Sethna 1988). Ayanle, Bernoff & Lichter (1990) applied the perturbation approach of Jones (1984) to derive the coupled nonlinear Schrödinger equations that describe the interaction of cross-wave modes near a codimension two point. The equations were projected onto a centre manifold and solved to find multimode steady-state and periodic solutions.

A single cross-wave mode is a standing wave with its crests parallel to the sides of the tank. The cross-wave mode number, $N$, can be easily identified by counting the number of half-wavelengths spanning the tank. A single mode can be unstable to slow streamwise modulations, and several modes can interact to produce spanwise modulations. In this paper, we report on the observations of cross-waves in a long channel parametrically forced by a wavemaker at one end. As a function of two parameters, forcing frequency and forcing amplitude, regions are found in which the modulations may produce a periodic, quasi-periodic, or chaotic temporal variation of wave height (§§3.1 and 3.2). The different types of motion are mapped out in parameter space and identified by their winding numbers (cf. §§1.2 and 2.2). At large forcing amplitudes, the spanwise modulation becomes localized into soliton-like pulses traversing the width of the tank. The sloshing soliton is not locked to the forcing frequency, resulting in a noisy periodic modulation (§3.3). Observations near the point of intersection of two adjacent neutral stability curves (§3.4) reveal a steady mixed-mode state previously described by Ayanle *et al.* (1990) using a set of coupled nonlinear Schrödinger equations.

The temporal features of the wave states are quantified by power spectra, Lyapunov exponent, correlation dimension, and winding number. Spatial structures are identified by multiprobe measurements and image processing.

Miles (1984) has shown that the motion of inviscid cross-waves is formally equivalent to a parametrically forced pendulum. The work presented here shows that more complicated states can be considered as weakly coupled oscillators and may be partially described (§4) using the theory of circle maps (MacKay & Tresser 1986).

The remainder of this paper is organized as follows. The theory of weakly coupled oscillators is presented in §1.2. The wave tank, experimental procedures, and methods of data processing are described in §2. The results are presented in §3. The experimental results are discussed and compared to the theory of three weakly coupled oscillators in §4. Also in §4, the observed steady mixed-mode state is compared to the multimode theory of Ayanle *et al.* (1990). The main conclusions are summarized in §5.

### 1.2. *Theory of weakly coupled oscillators*

The structure of the observed transitions is found to be similar to the behaviour of a system of weakly coupled oscillators. Below, the theory of weakly coupled oscillators and its relationship to circle maps are discussed. These ideas are compared with experiment in §4.

A natural setting for the description of a dissipative oscillator is a phase space in which one of the coordinates is the phase of the oscillator. When considering two oscillators, their phases yield coordinates on a torus. One can define a Poincaré section of this torus by sampling the motion at a fixed phase of one of the oscillators; the dynamics induce a circle map on the Poincaré section. Under appropriate conditions (Aronson *et al.* 1982) this mapping will be invertible and autonomous, and will reproduce the dynamics of the full system. The winding number, $w$, can then be

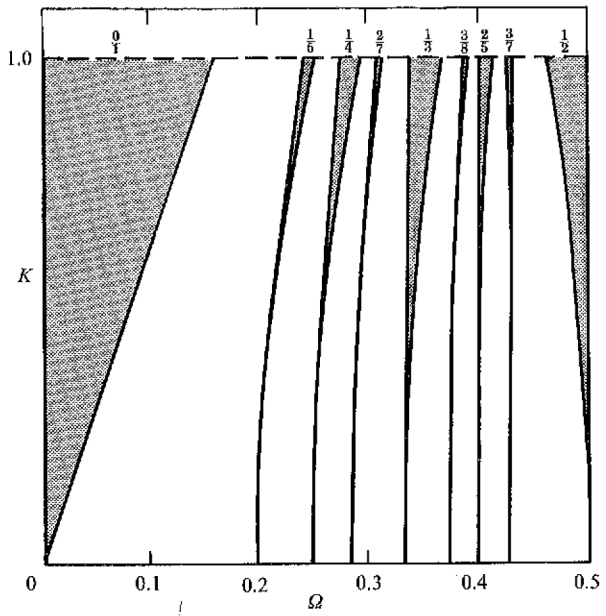


FIGURE 1. Arnold tongues for the circle map as a function of nonlinearity $K$ and frequency $\Omega$ (after Ecke *et al.* 1989). The shaded regions are frequency-locked tongues, which are marked with their winding numbers. The Farey sum of two winding numbers generates the winding number for an intermediate tongue. By repeatedly generating these sums, frequency-locked tongues between any two given tongues can be found. Only the largest tongues have been shown.

defined as the ratio of the number of times a trajectory wraps around the torus to the number of times it strikes the Poincaré section. It corresponds to the ratio of the frequencies of the oscillators. When the coupling of the oscillators is not weak, the circle map defined above may no longer faithfully model the behaviour of the full system (MacKay & Tresser 1986). The winding number in this situation may not converge to a unique limit.

A well-studied example (MacKay & Tresser 1986) is the sine (or standard) circle map,

$$\theta_{n+1} = \theta_n + \Omega + \frac{K}{2\pi}\sin(2\pi\theta_n) \mod(1),$$

where the iterates may be located on a circle of radius 1 by letting $2\pi\theta$ equal the circumferential angle. If $K = 0$, then the two oscillators are uncoupled, and the winding number is $\Omega$ (figure 1). When the nonlinearity $K > 0$, the two frequencies can lock to a fixed ratio over an interval of $\Omega$ corresponding to a rational winding number. The regions in $(\Omega, K)$ parameter space in which locking occurs are called Arnold tongues, or simply tongues. The tongues are widest (i.e. they persist for a wide interval of $\Omega$), and hence easiest to observe experimentally, when the ratio of the locked frequencies is equal to the ratio of two small integers. Between two tongues with winding numbers $p_1/q_1$ and $p_2/q_2$, a rational number with a larger denominator can be constructed by taking their Farey sum $(p_1+p_2)/(q_1+q_2)$; the resulting offspring is called the Farey daughter (Ecke, Farmer & Umberger 1989). By starting with the two fractions 0/1 and 1/1 and iterating this process, all rational numbers on the interval $(0, 1)$ can be constructed; this genealogical construction is

known as a Farey tree. For the circle map, this construction identifies Arnold tongues on progressively finer scales.

If the value of $\Omega$ is increasing at fixed positive $K$, the graph of the winding number will be a continuous non-decreasing function with finite intervals fixed at each rational number corresponding to the frequency-locked tongues. A point for each irrational winding number can also be found between the rational steps. This graph is known as a devil's staircase (Bak, Bohr & Jensen 1985). Owing to the finite accuracy of the measurements only a finite number of these intervals will be observed in any experiment.

Unfortunately, when three oscillators are considered, the dynamical picture exhibits much richer structure and is only poorly understood (Linsay & Cumming 1989; Cumming & Linsay 1988; Arneodo, Coullet & Spiegel 1983). The work of Newhouse, Ruelle & Takens (1978) suggests that chaotic behaviour will be observed with arbitrarily weak coupling. However, much of the ordered structure will persist, also. All three frequencies can lock in rational ratios over finite intervals of parameter space. Or, two of the frequencies may lock strongly in a particular region, and the interaction of this common frequency and the third frequency may act as two coupled oscillators. Experimentally, we will concentrate on observing these ordered states by measuring two winding numbers as described below.

## 2. Experimental apparatus and data processing

### 2.1. *Apparatus*

Experiments were performed in a rectangular tank 121 cm long, 30.9 cm wide, and 30 cm deep; the water depth was 25.8 cm (see figure 2). Complete details of the apparatus and experiment procedures can be found in Underhill (1990). A wave absorber was mounted at the far end of the tank to minimize reflections. Finite length effects are discussed in detail in Kit & Shemer (1989) and Underhill (1990). To verify that the observed resonances were not unduly influenced by the finite length of the tank, experiments were run for various tank lengths by means of a false wall. The frequency peaks were not seen to shift for reductions of tank length less than 10 cm. A plane wavemaker, hinged on a pedestal 11.7 cm from the bottom, was located 29 cm from one end of the tank. There was a gap of 0.075 cm between the wavemaker and the sidewalls. The wave field in the test section was influenced, via communication through this gap, by the waves and chop behind the wavemaker. These waves had a noticeable effect on the growth rate of the cross-waves. Therefore, the area behind the wavemaker was covered with a piece of soft sponge rubber, which prevented the growth of any waves behind the wavemaker. Decreasing the gap width had no measurable effect on the location of the neutral stability curves and other bifurcation curves.

The wavemaker was driven by a linear d.c. motor controlled by a Galil DMC-230 motion control system. A computer-generated sine wave of variable frequency and amplitude was converted to an analog signal and used as a reference signal to the controller. The reference was compared at $10^3$ Hz with the actual wavemaker position as monitored by an optical encoder that had a resolution of $2.0 \times 10^{-3}$ mm, and the closed-loop positioning feedback was updated to the motor. Frequency stability was within $10^{-4}$ Hz. The frequency was adjustable in increments of $2 \times 10^{-3}$ Hz and, by accessing the clock chip directly, could be changed while the waveform remained continuous. When modulations were present in the wave field, the wavemaker was subject to a varying hydrodynamic load. The motion control

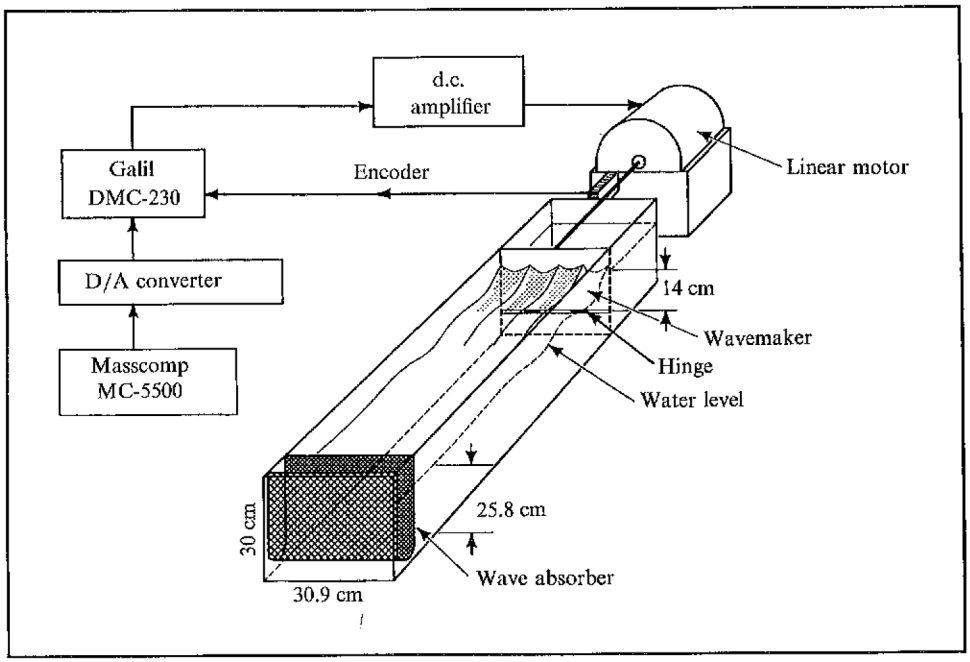


FIGURE 2. Schematic of the experiment. Details of the apparatus are given in §2.1.

system effectively excluded coupling of these loads to the motion of the wavemaker. Under the most extreme modulation conditions, the wavemaker amplitude fluctuated by less than 2%. Though the feedback to the wavemaker affected the extent of instability regions, the effect was slight (see §4).

Wave height was measured by a capacitance-type probe whose active element was a single length of insulated wire 0.2 mm in diameter. The capacitance of the wire varied linearly with the wave height. The probe was modified from a circuit supplied by Joe Hammack of the University of Florida. Static calibration of the probes showed a signal to noise ratio of 380/1. Phase and amplitude distortion were less than 3% for frequencies up to 20 Hz. While the probes were often as close as 1 cm to the wavemaker, they could be moved to a location up to 3 cm from the wavemaker if considerable wave breaking occurred.

Prior to conducting any experiments, the wave tank was filled with tap water and allowed to reach room temperature. Also, the surfactant Kodak Photo-Flo 200 (Wu, Keolian & Rudnick 1984) was added to attain a 0.6% concentration by volume. Experimental results were repeatable if the water was changed every 7 days and allowed to sit for at least a day after refilling. The surface tension at this concentration was the minimum attainable and equal to 33.8 dynes/cm as measured by the de Nouy ring technique (Chen 1987).

### 2.2. *Data analysis*

Takens (1981) showed that a single measurement of a $d$-dimensional flow can generally be used to reconstruct trajectories by looking at a $(2d+1)$-dimensional phase space constructed with time delays. In this case, the wave height, $A(t)$, at time $t$ was used to generate a coordinate vector

$$\xi(t) = \{A(t), A(t+\tau) \ldots A(t+(2d+1)\tau)\},$$

where $\tau$ is the time delay which is chosen to obtain a clear picture of the phase portrait. In practice, $\tau$ varied between a sixth and a third of the one-mode oscillation period. For the dimension measurements described below, the reconstructed phase space was, at most, six dimensional. Poincaré sections of the three-dimensional phase space were obtained by sampling at the subharmonic frequency.

The algorithm of Wolf *et al.* (1984) was used to compute the largest Lyapunov exponent. The Lyapunov exponents were measured in bits per unit time, the rate at which the error doubles. The method of Grassberger & Procaccia (1983) was used to measure correlation dimension. All algorithms were tested for several simple systems of known dimension and Lyapunov exponents, including the Hénon and Rossler attractors. The correlation dimension was measured for the Poincaré section, so the dimension in the full phase space is the measured value plus one.

Power spectra were performed using a standard fast Fourier transform algorithm, typically on 1024 points, sampled at the subharmonic frequency. The bandwidth was typically about 2 Hz, with a resolution of $4 \times 10^{-3}$ Hz.

When three intrinsic frequencies are locked in a periodic state, one can define two winding numbers. In this paper, winding number is used as a diagnostic to investigate locked states. If the motion is chaotic, the winding number may no longer be well defined. The winding number $w(F_1/F_2)$ relating the one-mode frequency $F_1$ and the sloshing frequency $F_2$ was determined by taking the ratio of the frequencies at the two spectral peaks. A more precise method for determining the winding number $w(F_0/F_2)$ ($F_0$ is the subharmonic frequency) was suggested by Charles Tresser (cf. Guckenheimer & Holmes 1983). It is assumed that the flow lies on or near some torus and that for each time a trajectory winds around the torus, its coordinates on the Poincaré section will have a unique maximum. If the number of times the trajectory strikes the Poincaré section between successive maxima is called $p_i$, then the number of times the trajectory strikes the Poincaré section per winding is approximated by

$$\omega_n = \frac{1}{n}\left(\sum_{i=1}^{n} p_i\right) \quad (n = 1, 2, 3, \ldots),$$

with an error of order $1/n$. Define

$$\Omega_{\min} = \lim_{N\to\infty} \inf_{n>N} \{\omega_n\},$$

and

$$\Omega_{\max} = \lim_{N\to\infty} \sup_{n>N} \{\omega_n\}.$$

If $\Omega_{min} = \Omega_{\max} = \Omega$, the winding number, $\Omega$, is well defined. If $\Omega$ is rational, the trajectory is approaching a limit cycle; if $\Omega$ is irrational, the motion is quasi-periodic. If $\Omega_{\max} > \Omega_{\min}$, the winding number is not uniquely defined and the motion is chaotic. In practice, only finite data sets were accumulated so, of course, $N$ was finite. At small forcing amplitudes, convergence was generally observed within 50 modulation cycles. Large forcing amplitudes had slower convergence rates, and as many as 200 modulation cycles had to be recorded.

Since the locking to the driver occurred with a winding number greater than 5 and the one-mode/sloshing occurred with a ratio less than or equal to 1, there should be no confusion; however, the distinction will be made precise by explicit use of $w(F_0/F_2)$ or $w(F_1/F_2)$.

Two methods of determining the transverse spatial structure of the cross-wave envelope were used. In the first, a videotape of the cross-wave was taken with the

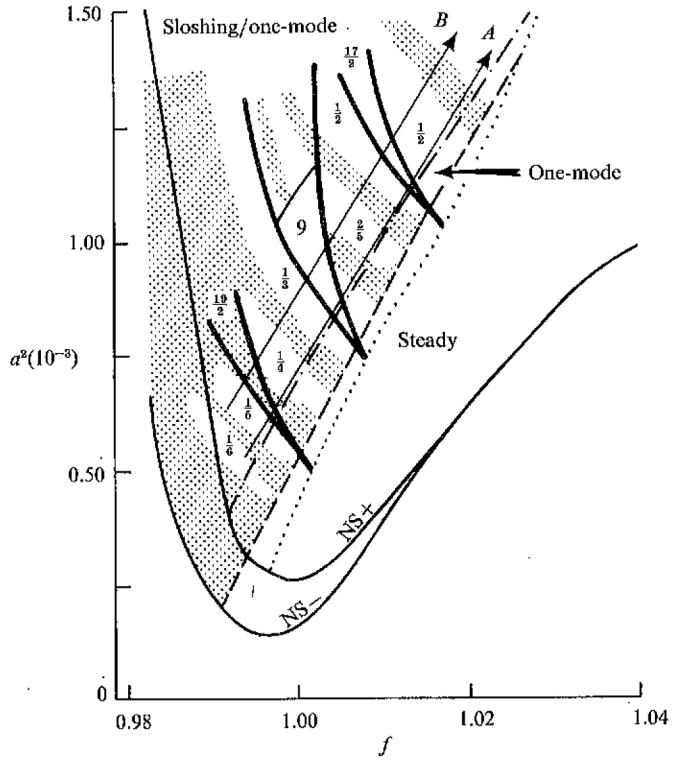


FIGURE 3. The parameter space near the resonant frequency for mode $N = 5$. Subharmonic tongues are bordered with a heavy line and labelled with the winding numbers $w(F_0/F_2) = \frac{19}{2}$, 9 and $\frac{17}{2}$. Quasi-periodic tongues are labelled with the ratio $w(F_1/F_2)$ of the one-mode frequency to the sloshing frequency. The neutral stability curve is labelled NS+; owing to a hysteretic subcritical bifurcation, cross-waves can persist to the lower transition NS−. The transition from a steady cross-wave to a one-mode modulation occurs across the dotted line. The transition to sloshing is hysteretic; it first occurs for increasing forcing amplitude on crossing the dot-dashed line and persists for decreasing forcing amplitudes to the dashed line. Chaotic regions are stippled. The ratio $w(F_1/F_2)$ measured along the line $A$ is shown in figure 5. The winding number $w(F_0/F_2)$ along the lines $A$ and $B$ is shown in figure 6. Within the tip of the $w(F_0/F_2) = \frac{19}{2}$ tongue, the one-mode oscillation is barely present; its amplitude begins to increase rapidly on crossing the diagonal line within the tongue (cf. figure 11).

camera's line-of-sight nearly horizontal and the lighting arranged to minimize direct reflections to the camera and to make the wave field as dark as possible relative to the white wavemaker. The image was stored on $\frac{3}{4}$-inch video tape at 30 frames/s and then digitized and transferred to floppy disk. An edge-finding program, developed by Robin Strickland of The University of Arizona, Department of Electrical and Computer Engineering, determined the surface profile at the wavemaker at 512 points and performed a Fourier decomposition. While this method worked well, it was more expedient to use the multiprobe method of Simonelli & Gollub (1988). For an $n$-probe array, the Fourier amplitude of $n$ modes can be determined by assuming the signal is a linear superposition of these modes and inverting the corresponding $n$-dimensional linear system. In practice, image processing was first performed to determine the number, $n$, of active modes in a particular state. The $n$-probe technique was then used to explore the time history of the state in detail.

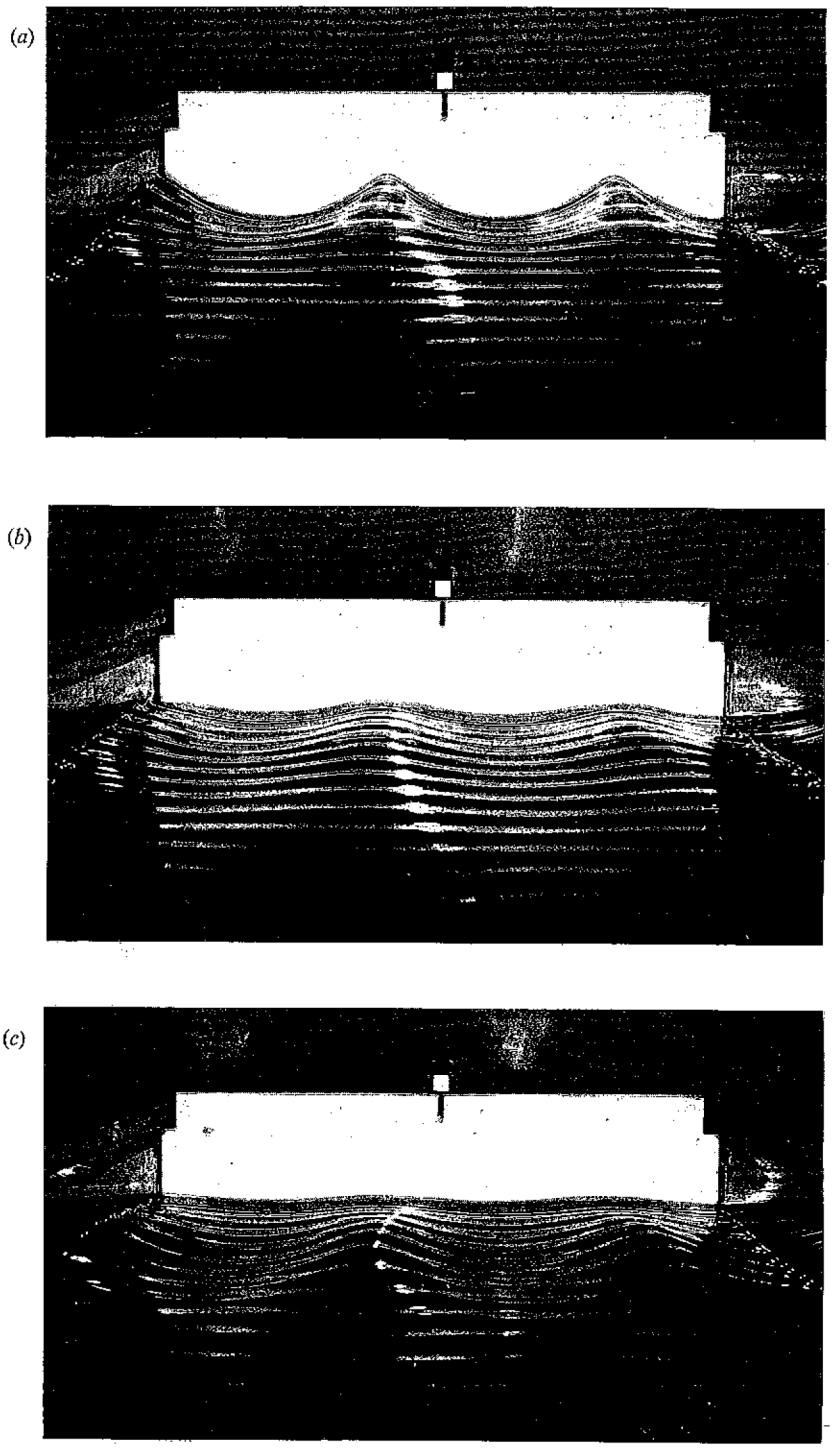


FIGURE 4. Photographs of the two types of slow modulation, for mode $N = 5$. The view is towards the wavemaker from the end of the channel. The one-mode modulation is shown over half a modulation period $T_1 = 1/F_1$ at the approximate times (*a*) $t = 0$, (*b*) $t = \frac{1}{4}T_1$ and (*c*) $t = \frac{1}{2}T_1$. The dimensional modulation period is about 15 s. Note that the peak amplitude is constant across the width of the tank. In (*c*), the peak amplitude has progressed away from the wavemaker.

(*d*)

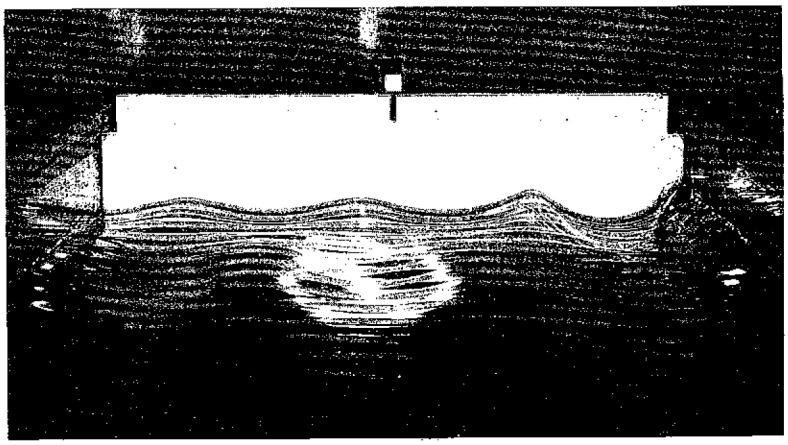

(*e*)

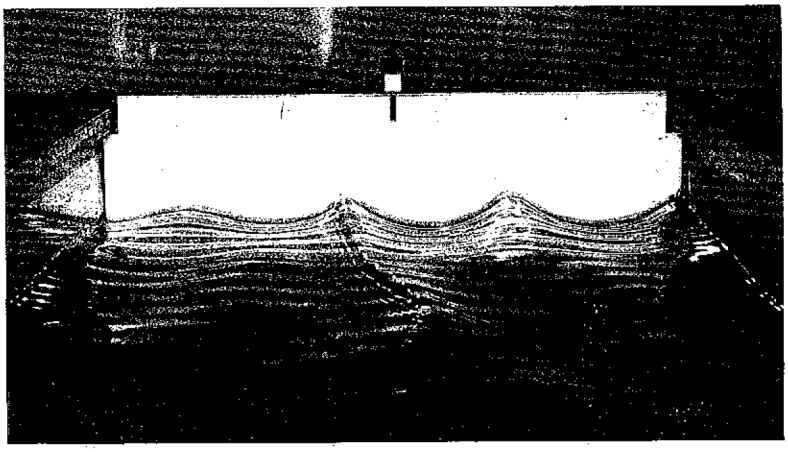

(*f*)

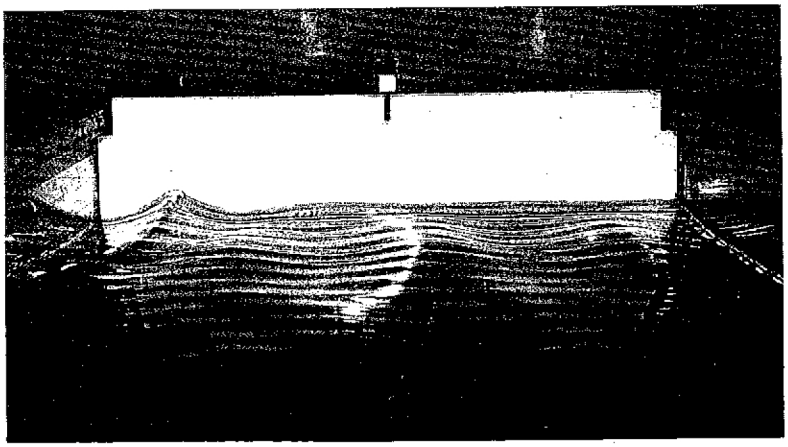

The sloshing modulation is shown at the approximate times (*d*) $t = 0$, (*e*) $t = \frac{1}{4}T_2$ and (*f*) $t = \frac{1}{2}T_2$, where the modulation period $T_2 = 1/F_2$. The dimensional modulation period is about 1.5 s. At the beginning of the modulation period (*d*), the wave amplitude has a peak on the right wall. The modulation propagates to the centre of the tank (*e*), and is then reflected from the left wall (*f*).

## 3. Results

Experiments were performed over a range of forcing frequencies $7.0 < \hat{f} < 9.0$ Hz, which covered the proximity of the resonant frequencies for modes $N = 5$, 6 and 7 ($\hat{f}_N = 7.12$, 7.82 and 8.46 Hz, respectively). The results for each mode number are presented in non-dimensional units based on the cross-wave wavenumber, $\hat{k}_N$, and resonant frequency, $\hat{f}_N$. The non-dimensional frequency, $f = \hat{f}/\hat{f}_N$, equals 1 at resonance (Jones 1984), and the lengthscales and timescales are non-dimensionalized by multiplying by $\hat{k}_N$ and $\hat{f}_N$, respectively. Forcing amplitudes, $a$, were as large as three times the minimum forcing amplitude necessary to maintain cross-waves. Lichter & Bernoff (1988) found that in the inviscid limit all bifurcations of a single mode appear as straight lines on the stability diagram when the coordinates $(f, a^2)$ are used. These coordinates are therefore adopted here.

Two distinct types of slow periodic modulations of the cross-wave field were observed. The interactions of these two types of modulation with each other and with the forcing frequency created the structure of parameter space that will be described in this section.

Figure 3 shows the parameter space near the cutoff for mode $N = 5$. On increasing the forcing amplitude at fixed frequency, cross-waves first appeared on traversing the neutral stability curve (NS+). This curve has been the object of many studies since Barnard & Pritchard (1972), most recently by Shemer & Lichter (1990). Once formed, cross-waves persisted on decreasing the forcing amplitude to the lower hysteretic transition (NS−) as described in Lichter & Bernoff (1988). The steady cross-wave lost its stability on crossing the line denoted by dots to a modulated standing wave whose amplitude envelope across the width of the tank was uniform, but grew and decayed with a low frequency $F_1$, which may be as much as two orders of magnitude less than the forcing frequency $f$. This state is well known from the experiment of Barnard & Pritchard (1972): 'After the cross-wave amplitude has passed through a maximum, a wave detaches itself from the wavemaker, propagates along the channel and is eventually absorbed at the beach' (as shown in figures 4*a–c*). The observation is described by the theory for a single spatial mode (Lichter & Chen 1987). Hence, we call this the one-mode oscillation.

The second type of modulation appeared on crossing the dot-dashed line in figure 3 as the forcing amplitude was further increased. This modulation was characterized by a transversely propagating wave (or waves) sloshing from side to side in the tank, causing the peak wave height to vary across the width of the tank. The transition to sloshing was hysteretic; once excited, the sloshing waves persisted down to the lower forcing amplitude marked by a dashed line. The sloshing frequency $F_2$ was greater than or equal to the one-mode modulation frequency $F_1$, and after transition (—·—), the amplitude of the sloshing field continued to be modulated at the lower one-mode frequency. Figures 4(*d–f*) show the typical appearance of the sloshing modulation. The sloshing modulation is discussed further in §3.3. Figure 5 shows the ratio of the one-mode frequency to the sloshing frequency $w(F_1/F_2)$ along path $A$ in figure 3. The winding number $w(F_0/F_2)$ along paths $A$ and $B$ is shown in figure 6. The frequency-locked intervals along curve $B$ were shifted with respect to those along $A$ due to the orientation of the tongues. The frequency-locked regions of the parameter space shown in figure 3 were mapped out from figures such as 5 and 6.

The band in which the one-mode modulation appeared alone (without the sloshing mode) was interrupted by the narrow tips of frequency-locked tongues, which extend into the one-mode region from the sloshing region (figure 3). The one-mode

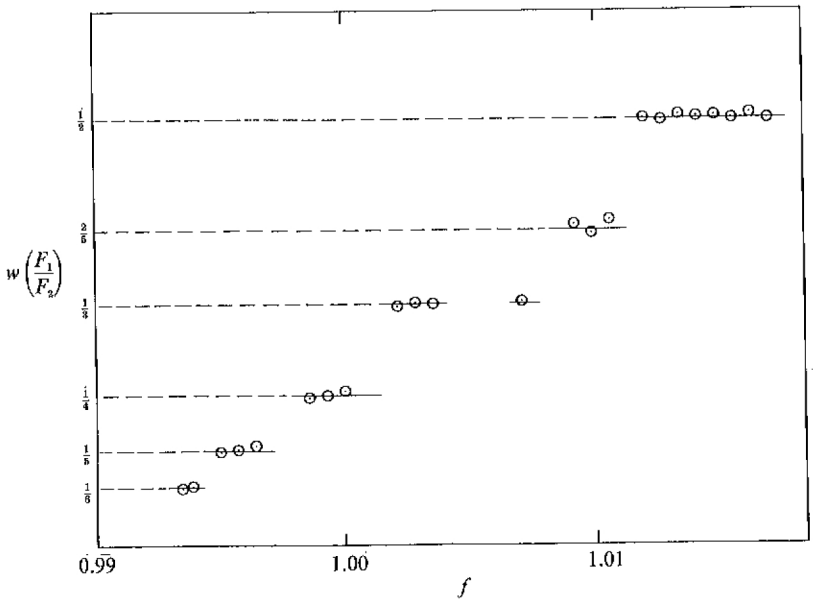


FIGURE 5. The ratio $w(F_1/F_2)$ of the one-mode modulation frequency $F_1$ to the sloshing frequency $F_2$ along path $A$ for forcing frequencies $f$ near the resonant frequency for mode 5 (cf. figure 3). The gap in the data at $w(F_1/F_2) = \frac{1}{3}$ is due to the tip of the $w(F_0/F_2) = 9$ subharmonic tongue for which the one-mode modulation is absent (cf. figure 11).

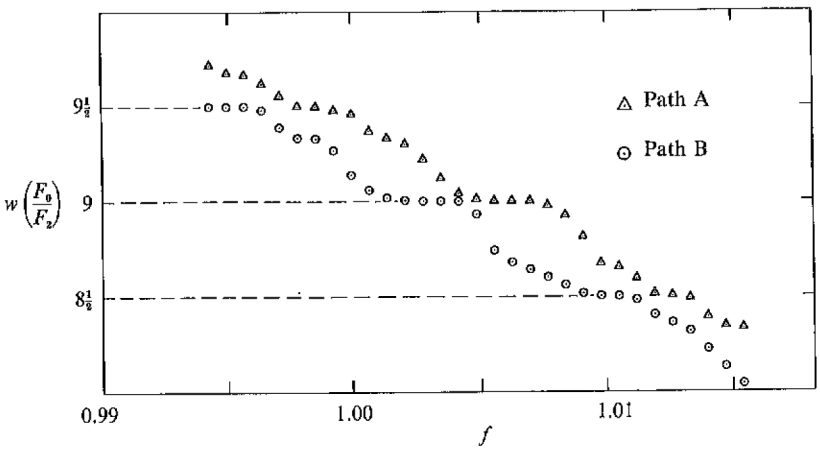


FIGURE 6. The winding number $w(F_0/F_2)$ as a function of forcing frequency $f$ along paths $A$ and $B$ for forcing frequencies $f$ near the resonant frequency for mode $N = 5$ (cf. figure 3).

modulation may be absent in the tips of these tongues (cf. §3.1). Within the tongues, the sloshing modulation was locked to the subharmonic frequency. These will be called subharmonic tongues. The three observed subharmonic tongues shown in figure 3 have winding numbers $w(F_0/F_2) = \frac{17}{2}$, $\frac{9}{1}$ and $\frac{19}{2}$.

Outside these subharmonic tongues were other tongues in which the sloshing was locked to the one-mode modulation but unlocked to the subharmonic frequency. Hysteresis was not observed in the neighbourhood of the boundaries of these tongues. However, perturbing the parameter across a boundary led to long transients before the transition was observed. These tongues are labelled with the ratio $w(F_1/F_2)$

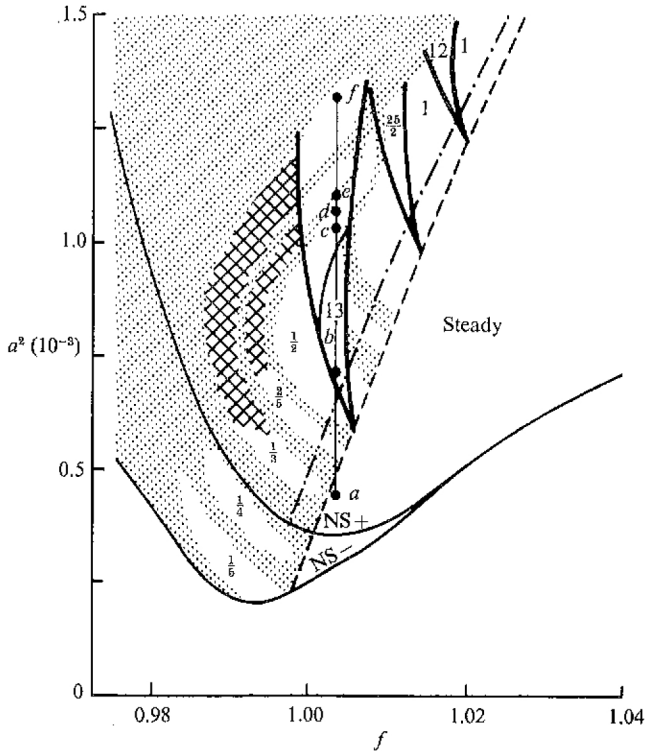


FIGURE 7. Parameter space near the resonant frequency for mode $N = 7$. The notation is as in figure 3. In addition, the cross-hatching denotes chaotic extensions of the quasi-periodic tongues. Though the wave height is chaotic within these regions, $w(F_1/F_2)$ remains equal to the value shown in the quasi-periodic part of the tongue. The points ($a$–$f$) along the line at $f = 1.004$ were investigated using power spectra (figure 8), Poincaré sections (figure 9), and largest Lyapunov exponent and correlation dimension (figure 10).

for the one-mode/sloshing frequencies and will be called quasi-periodic tongues because they were not locked to the subharmonic frequency. The quasi-periodic tongues observed had winding numbers $\frac{1}{6}$, $\frac{1}{5}$, $\frac{1}{4}$, $\frac{1}{3}$, $\frac{2}{5}$ and $\frac{1}{2}$. Regions in which the wave height was apparently chaotic were between the tongues.

Where the quasi-periodic tongues overlapped the subharmonic tongues, states were observed where all three frequencies were locked. Areas of chaos were seen between these triply locked regions.

Near the resonant frequency for other mode numbers, the regions of chaos and mode locking were similar (figure 7). However, there were differences dependent on mode number. It appeared as if the one-mode band became thinner as the mode number increased. For $N > 6$, the one-mode modulation was never stable and the uniformity of the cross-wave envelope would, within a minute of the onset of modulation, be augmented by a sloshing mode. Hence, there was no band for $N = 7$ in figure 7 that corresponded to that in figure 3 for $N = 5$, in which the one-mode oscillation existed without the simultaneous presence of the sloshing mode.

The parameter space near the cutoff for mode 7 will now be discussed in greater detail, as it was the region where the most extensive measurements were taken.

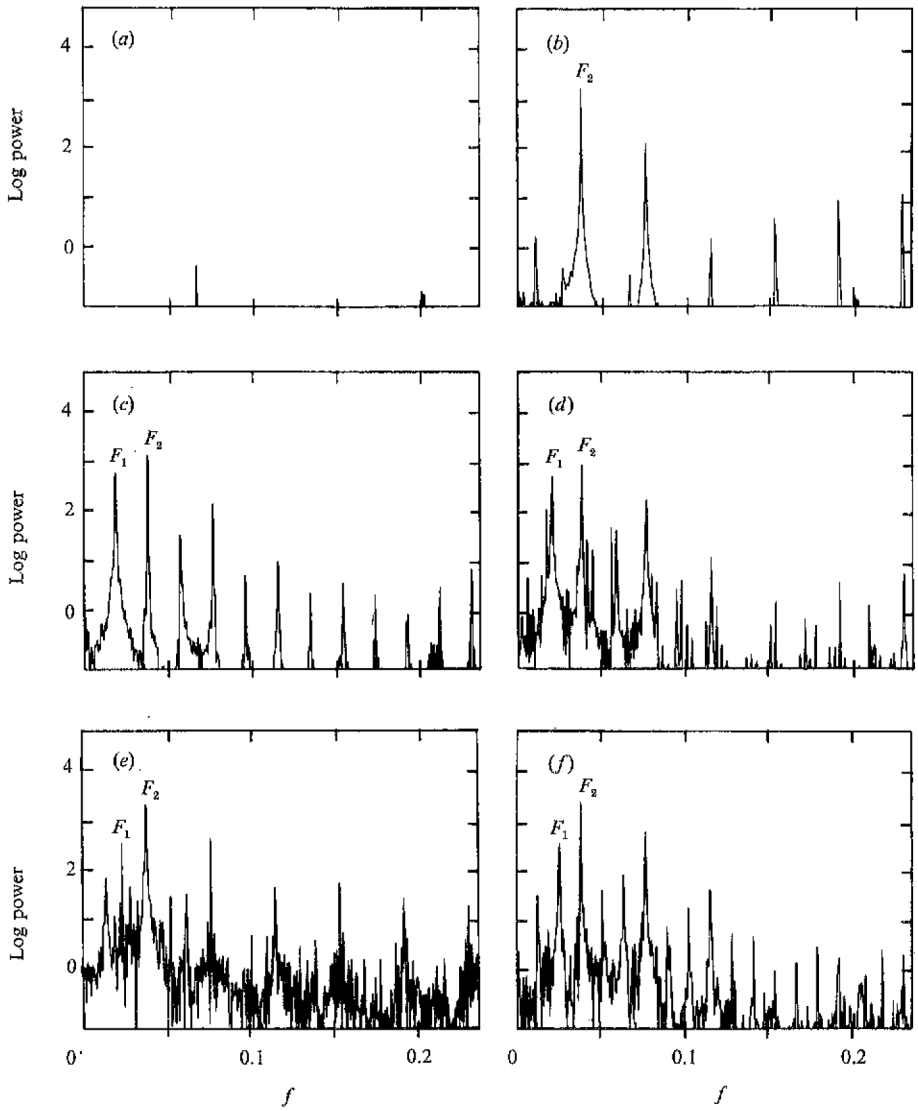


FIGURE 8. Power spectra for the points shown in figure 7 along the line at $f = 1.004$ within the subharmonic tongue. The corresponding Poincaré sections are shown in figure 9. The spectral peak at the subharmonic frequency has been removed by sampling each subharmonic period. (*a*) The steady cross-wave. (*b*) In the tip of the tongue. The one-mode oscillation, $F_1$, is relatively small. The sloshing, $F_2$, is locked to the subharmonic frequency in a ratio $w(F_0/F_2) = 13$, creating 13 periodic points. (*c*) On crossing the diagonal line interior to the tongue, the one-mode oscillation appears. (*d*) The one mode oscillation is incommensurate with the subharmonic, forming 13 loops in the Poincaré section, one each around the former locations of the 13 periodic points. (*e*) In the chaotic band. (*f*) The $w(F_1/F_2) = \frac{2}{3}$ frequency-locked region.

### 3.1. *Subharmonic tongues*

If the steady cross-wave was unmodulated (figure 8*a*), then its Poincaré section was simply a fixed point in phase space (figure 9*a*). The $w(F_0/F_2) = 13$ subharmonic tongue was explored by commencing with the steady state and then observing a sequence of states along the line at $f = 1.004$ (figure 7). Near the tip of the tongue, the Poincaré section visited each of 13 fixed points for each modulation period (figure

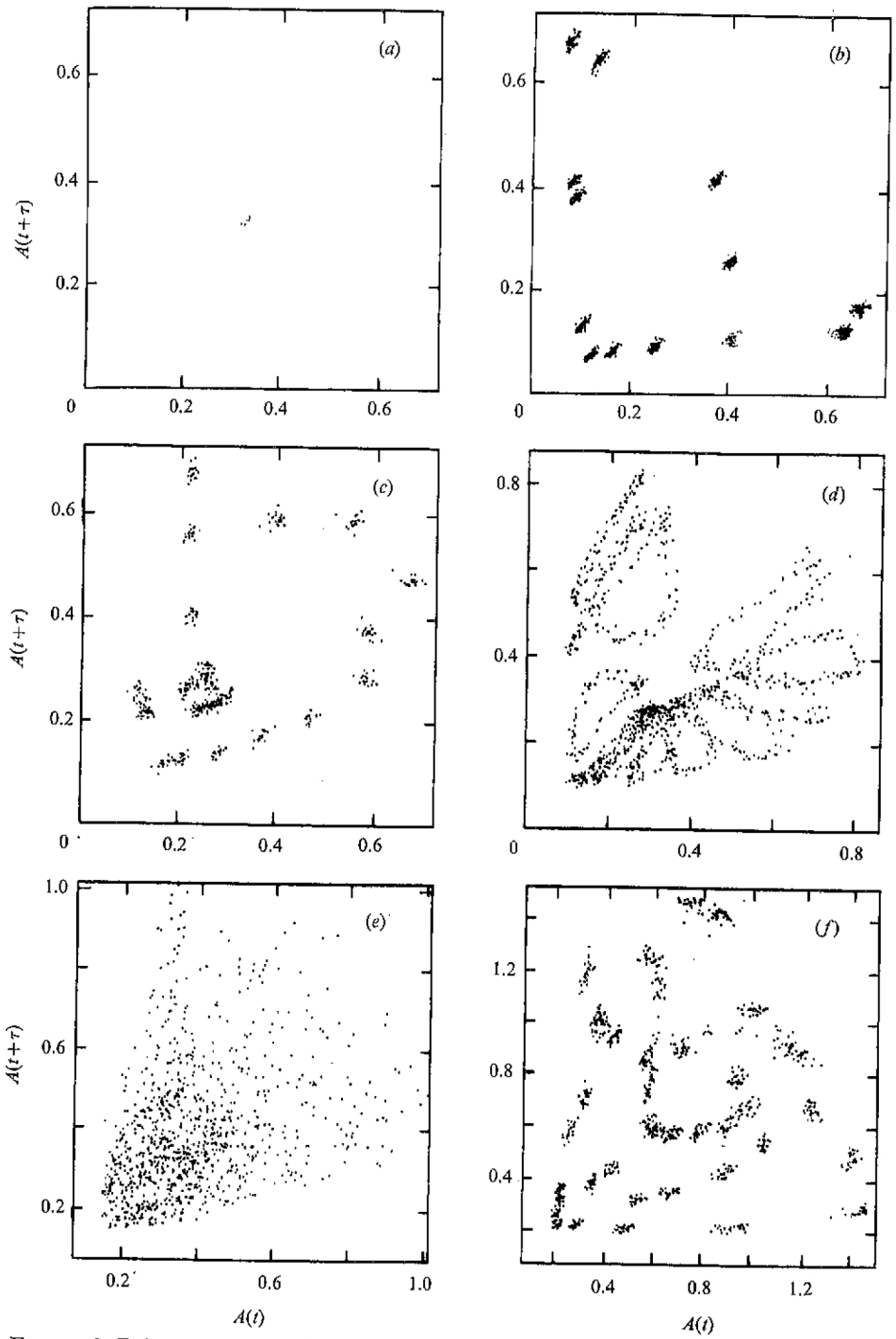


FIGURE 9. Poincaré sections for the points *a–f* shown in figure 7 and described in the caption for figure 8. $A(t)$ is the wave height.

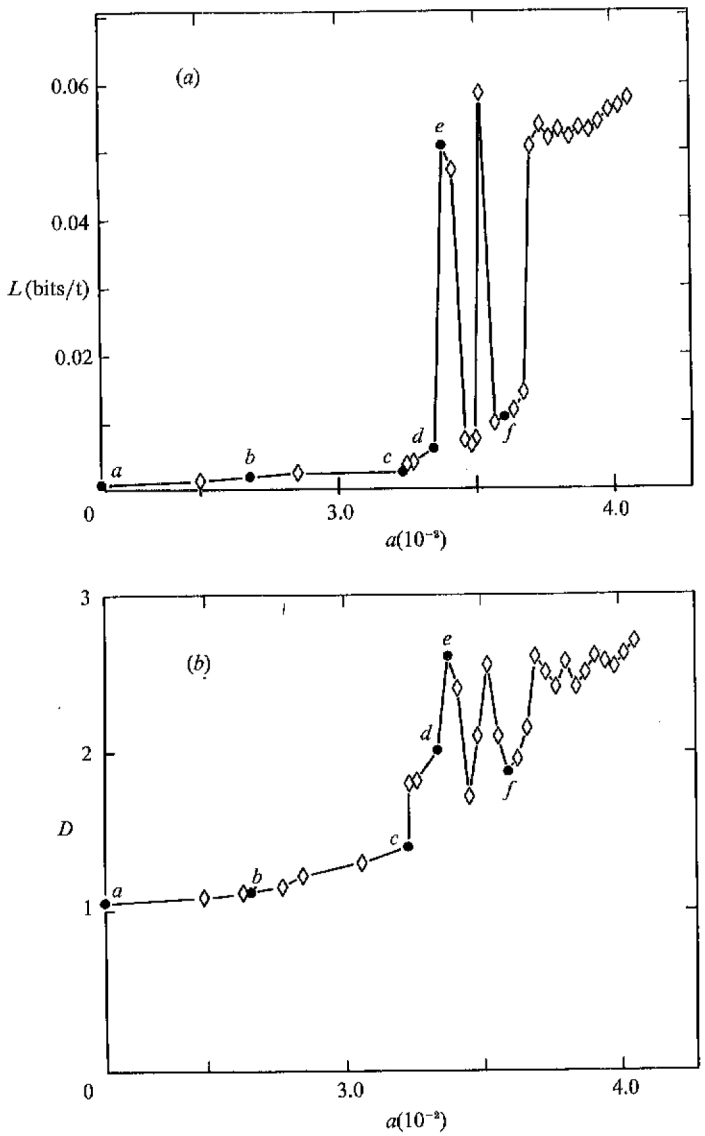


FIGURE 10. Largest Lyapunov exponent ($a$) and correlation dimension ($b$) as a function of forcing amplitude at constant $f = 1.004$. The labelled points ($a$–$f$) refer to the points shown in figures 7, 8 and 9.

9$b$). The largest Lyapunov exponents (figure 10$a$) for both the steady state and modulated state were very small, $< 2.4 \times 10^{-3}$ bits/time (here, bits/time measures the rate at which error doubles, cf. §2.1). The correlation dimensions (figure 10$b$) were near unity. The one-mode modulation was discernible in the tip of this tongue, but was barely above the noise level; there was only a small one-mode peak in the spectrum (figure 8$b$). On crossing the diagonal solid line shown within the tongue, the one-mode modulation quickly grew (figures 8$c$ and 9$c$) at the frequency corresponding to one-half of the sloshing modulation (figure 11). Though the one-mode oscillation was present with minimal amplitude below this line, it increased rapidly at larger amplitudes, as discussed at the end of this section. The region occupied by

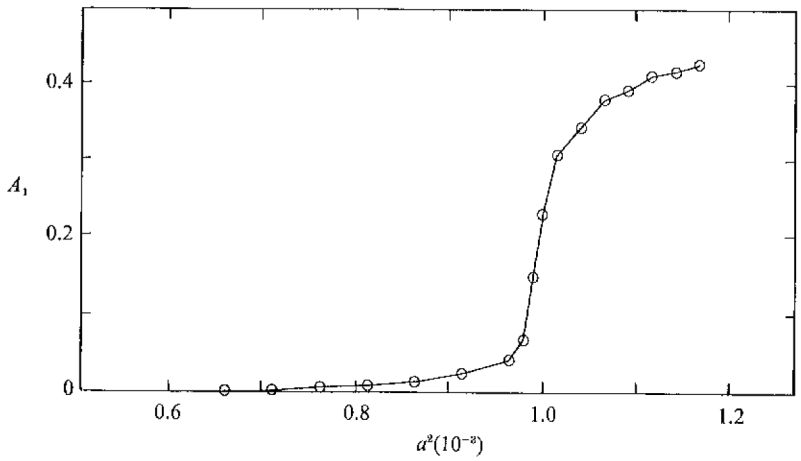


FIGURE 11. Amplitude $A_1$ of the one-mode amplitude versus forcing amplitude squared, $a^2$, at forcing frequency $f = 1.004$ within the $w(F_0/F_2) = 13$ subharmonic tongue. The amplitude $A_1$ was determined from power spectra by taking the square root of the amplitude of the spectral peak at frequency $F_1$.

the one-mode plus sloshing modulation is marked by $w(F_1/F_2) = \frac{1}{2}$. There was no evidence of a cascade of period doublings following this state; instead, on further increase of the forcing amplitude, the periodic fixed points lost their stability as the one-mode frequency became incommensurate with the sloshing frequency. When the frequency is incommensurate, the phase portrait is expected to be a torus. The iterates of the Poincaré section (figure 9*d*) hopped from loop to loop, each loop corresponding to a cross-section of the torus. Each loop was circumnavigated with a frequency $2F_1 - F_2$, which appeared as the lowest frequency peak in figure 8(*d*). The evolution to the chaotic state (figures 8*e* and 9*e*) was accompanied by abrupt increases of the Lyapunov exponent to $5.1 \times 10^{-2}$ bits/time and the correlation dimension to 2.45 (figure 10). The chaotic states constituted a narrow band and, at larger forcing amplitudes, a non-chaotic region appeared in which $w(F_1/F_2) = \frac{2}{5}$. Associated with this region was a decrease of the Lyapunov exponent to near zero and a decrease of the dimension to below two. On further increasing the forcing amplitude, the modulations again became aperiodic, chaotic motion reappeared, and the Lyapunov exponent and correlation dimension increased abruptly. This band of chaos lies below a region for which $w(F_1/F_2) = \frac{2}{3}$ (figures 8*f* and 9*f*). At even higher forcing amplitudes, a chaotic region reoccurred. These large forcing amplitudes will be discussed in §3.3.

Near the tip of the tongue, sloshing occurred without being accompanied by the one-mode oscillation. Three probes were used to measure the amplitude of the odd and even components of the cross-wave (figure 12). A probe at the centre of the tank gave the amplitude of the even mode, while the odd mode amplitude was the difference of the measurements from two probes symmetrically phased at the nodes closest to the centreline of $N = 6$; this placement maximizes the ratio of the odd to even mode amplitudes. Note that the amplitude of the even modes changed sign. The portrait was nearly symmetric with respect to a change of sign of the even modes. A slight asymmetry was due to the odd number of subharmonic periods in the sloshing period. As we continued through the tongue, the amplitude of the one-mode oscillation rapidly increased. This corresponded to the destruction of the symmetric

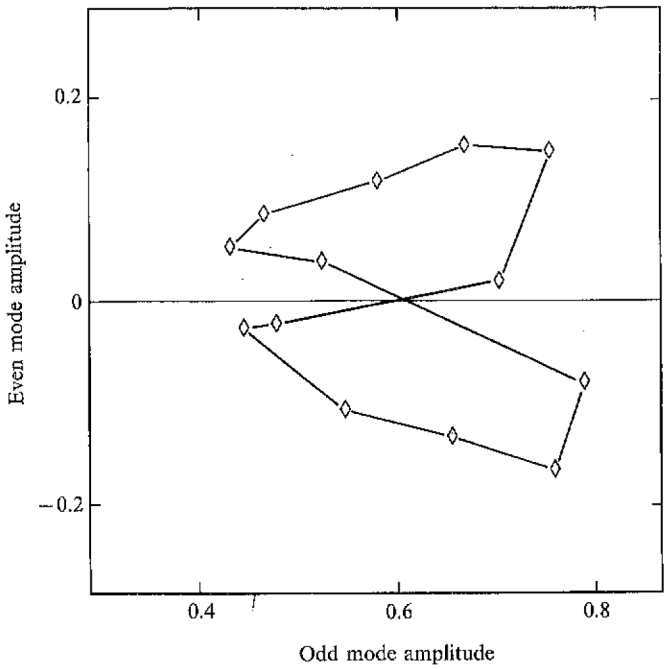


FIGURE 12. Phase plane portrait of the even and odd components of the wave height of the sloshing wave within the tip of the $w(F_0/F_2) = 13$ tongue (figure 7). The asymmetry is due to the odd number of subharmonic cycles for one complete sloshing modulation period.

character of the phase portrait. In the discussion, this will be related to an imperfect symmetry-breaking bifurcation.

### 3.2. *Quasi-periodic tongues*

Outside and overlapping the subharmonic tongues were quasi-periodic tongues in which the sloshing frequency was locked to the one-mode frequency but unlocked to the subharmonic (figures 3 and 7). Between these tongues were chaotic regions that widened to fill the parameter space at large forcing amplitudes and negative detunings. The cross-hatched regions in figure 7 are chaotic regions characterized by the presence of a second transverse wave (§3.3). However, the cross-hatched regions can be considered as extensions of the quasi-periodic tongues. Although there was an increase in the noise level moving up through the cross-hatched region, the spectral peaks for the one-mode and sloshing frequencies were still narrow and $w(F_1/F_2)$ was equal to the value observed within the non-chaotic lower portion of the tongue. Continuing to higher forcing amplitudes, one of the intermediate spectral peaks may gain ascendancy; for example, within the cross-hatched region originating in the quasi-periodic $w(F_1/F_2) = \frac{2}{5}$ tongue, we sometimes found $w(F_1/F_2) = \frac{3}{6}$. And, finally, when the extension of the tongue neared the subharmonic tongue, we found only $w(F_1/F_2) = \frac{3}{5}$. The overlap of the quasi-periodic tongues with the subharmonic tongues will be discussed further in §4.

### 3.3. *Sloshing and noisy periodic modulations*

As the cross-wave amplitude was increased, the sloshing modulation dominated the dynamics of the motion. Several distinct sloshing states can be identified.

For small forcing amplitudes ($a^2 < 2.0 \times 10^{-3}$), the sloshing may consist of one or two transverse waves. For frequencies $f \gtrsim 1.00$, the sloshing appeared as a single wave traversing the tank from side to side. For frequencies $f \lesssim 1.00$, a second transverse wave appeared. Near $f \approx 1.00$, the two waves were difficult to distinguish. As the frequency was further decreased, the waves became easier to identify and were observed to pass through each other on alternate sides of the tank. The power spectra of the chaotic regions, including the areas shown cross-hatched (figure 7), were characterized by high noise levels. On traversing the neutral stability curve NS+, the two waves obtained their greatest separation and crossed repeatedly near the channel centreline. Between the curves NS+ and NS− (figure 7), the power spectra of the chaotic regions possessed a clearly defined peak at the sloshing frequency, though with a broad one-mode peak. In the chaotic regions, the one-mode frequency increased as a function of forcing frequency, as occurred within the sequence of quasi-periodic tongues.

At larger forcing amplitudes ($a^2 > 2.0 \times 10^{-3}$), two states were found for which the spectral peak at the sloshing frequency was accompanied by a high level of background noise (figure 13). We call these states 'noisy periodic'. For one of the states, two waves were again observed traversing the tank in opposite directions, repeatedly crossing at the centreline of the tank. A time series and power spectrum are shown in figures 13($a$, $c$). The second noisy periodic state appeared to consist of three travelling waves separated by $\frac{2}{3}$ of the tank width. A time series and power spectrum are shown in figures 13($b$, $d$).

### 3.4. *Near the codimension-two point*

The region in parameter space near the intersection of the neutral stability curves for modes $N = 6$ and 7 is shown in figure 14. The up-triangles mark the neutral stability curve for $N = 6$; this is a supercritical bifurcation to a steady cross-wave. The down-triangles mark the neutral stability curve for $N = 7$; this transition is subcritical and hysteretic. Upon crossing this boundary, an abrupt transition to a chaotic cross-wave was seen. The crosses mark the non-hysteretic transition from a steady mode $N = 6$ to a steady mixed-mode state of mode $N = 6$ plus mode $N = 7$. Figure 15($a$–$d$) shows the modal amplitudes of modes $N = 6$ and 7 as determined from multiprobe measurements (cf. §2.3). Point $a$ in figure 14 is a fixed point for mode $N = 6$, and the amplitude for mode $N = 7$ is nearly zero (figure 15$a$). Point $b$ is a fixed mixed mode in which both nodes $N = 6$ and $N = 7$ were present in proportions that were independent of time (figure 15$b$). This mixed mode appeared as a 'frozen' sloshing wave in which the modes were in phase on one side of the tank, producing a large cross-wave amplitude, and out of phase on the other side, yielding a small cross-wave amplitude. The contribution of mode $N = 7$ was always less than that of mode $N = 6$, but it increased with increasing frequency (point $c$, figure 15$c$). As the amplitude of mode $N = 7$ became equal to that of mode $N = 6$, the wave field became unstable and there was a transition to a chaotic wave field (point $d$, figure 15$d$). Transition to a chaotic wave field occurred at the points marked by the open circles in figure 14. The boundary is approximately the extension of the neutral stability curve from mode $N = 6$. The transition was irreversible since the steady-mixed mode could not be regained from the chaotic state.

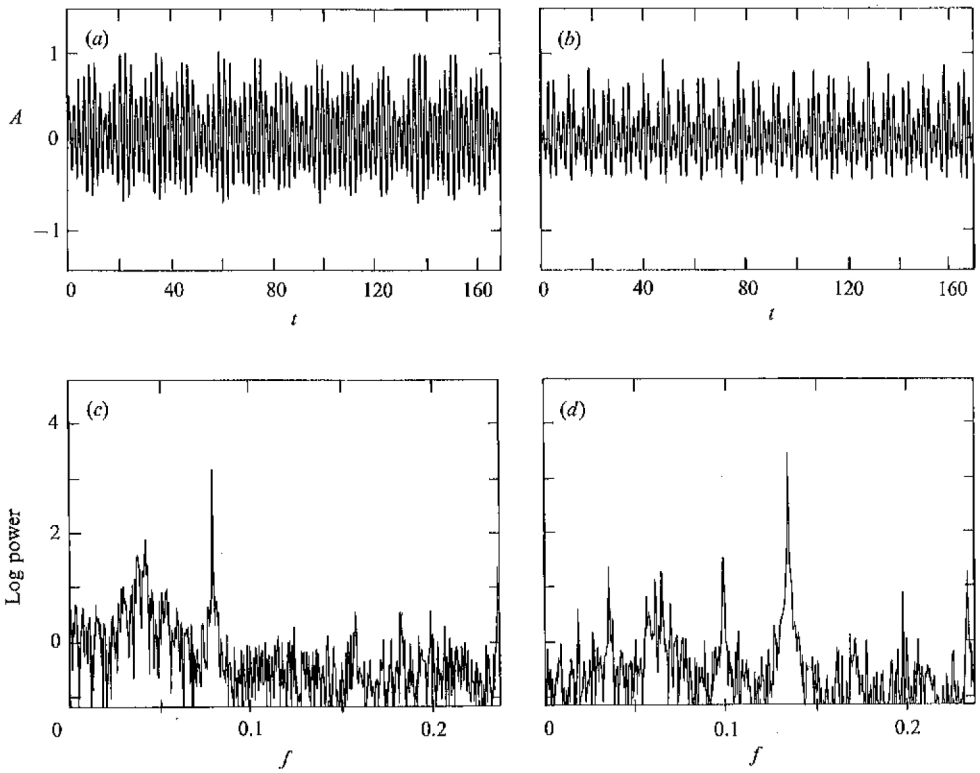


FIGURE 13. Noisy periodic modulations. Time series of wave height $A(t)$ for ($a$) two waves crossing at the channel centreline, $f = 1.00$ and $a^2 = 2.28 \times 10^{-3}$; and ($b$) three waves separated by $\frac{2}{3}$ of a tank width, $f = 1.02$ and $a^2 = 2.53 \times 10^{-3}$. Power spectra for the two-wave ($c$) and three-wave ($d$) cases.

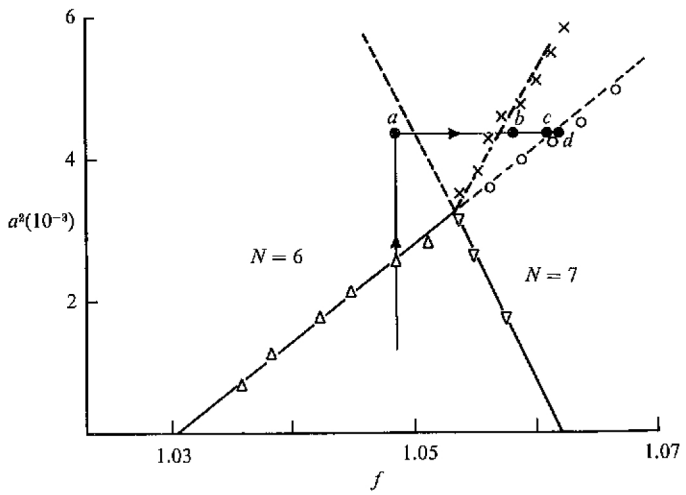


FIGURE 14. The mixed-mode state for modes $N = 6$ and 7. The up (down) triangles mark the neutral stability curve for mode $N = 6$ ($N = 7$). The crosses mark the transition to the mixed mode. The circles mark the transition to the chaotic state. The arrowhead on the line indicates the direction that a path must take in order for the mixed-mode state to be found. The points $a$–$d$ correspond to figure 15($a$–$d$). The non-dimensional frequency $f$ and amplitude $a$ are based on $f_6$ and $k_6$, respectively.

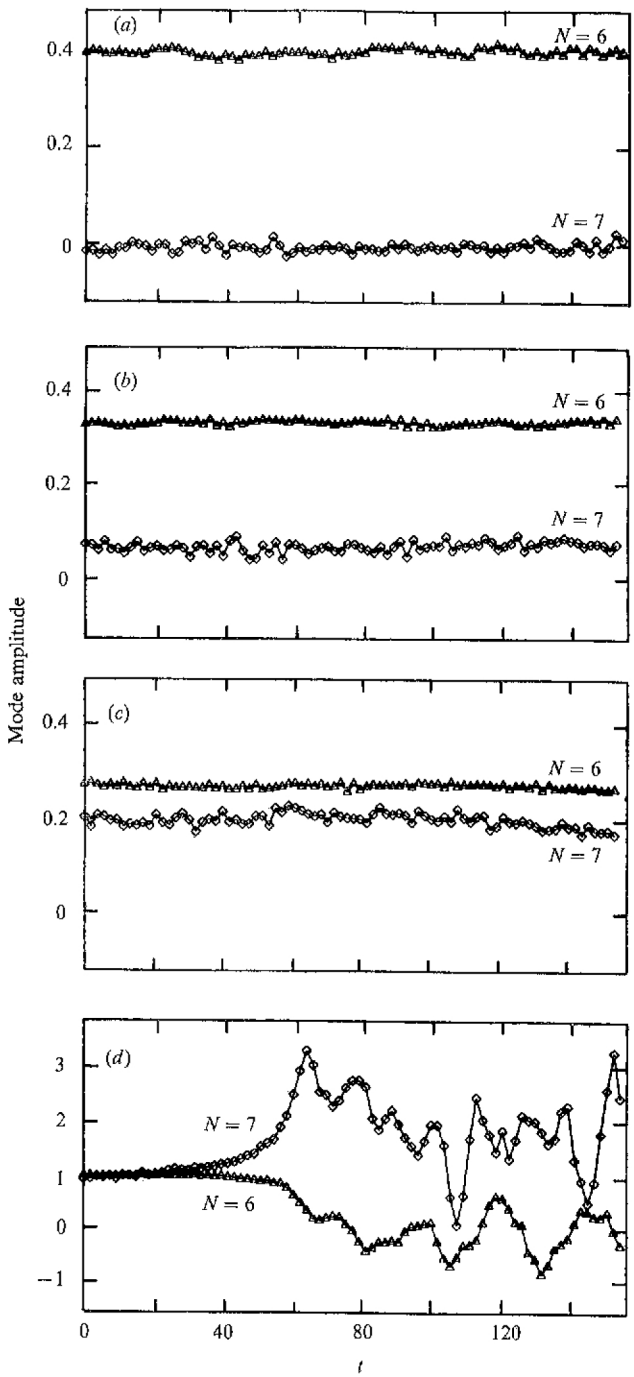


FIGURE 15. The amplitudes for modes $N = 6$ and 7 as determined using the two-probe technique described in §2.2. The figures correspond to the points *a–d* in figure 14 as forcing frequency $f$ is increased at fixed forcing amplitude $a^2 = 1.23 \times 10^{-3}$. (*a*) The fixed point for mode $N = 6$. Mode $N = 7$ is nearly absent. (*b*) A mixed-mode state with some mode $N = 7$. (*c*) As in (*b*) but the contribution of mode $N = 7$ has increased. (*d*) The transition to a chaotic state. Note that mode $N = 6$ is beginning to oscillate about a zero mean, characteristic of one type of sloshing (cf. figure 12). The non-dimensional time $t$ and amplitude $a$ are based on $f_6$ and $k_6$, respectively.

## 4. Discussion

Van Atta & Gharib (1987) document a case in which vibrations of a supposedly stationary cylinder rendered a study of fluid instability to one of solid–fluid interaction. This interaction produced artifactual regions of chaos that were not present in the fluid system alone. To guard against the possibility that, in our system, the observed bifurcation structure was a result of interaction with the wavemaker, the positions of the poles of the motion controller's transfer function were moved, changing the response characteristics of the wavemaker. However, the frequency-locked tongues remained in the same regions in parameter space. Additionally, the feedback gain of the motion control system was reduced from its usual setting to a low value. Once again, the frequency-locked tongues still appeared in the same regions of parameter space. It was also observed, as would be expected, that the width of the tongues was reduced due to the stochastic variations of the forcing amplitude (Funakoshi & Inoue 1988).

The location of the neutral stability curves (NS+/−) and the transition curve to the one-mode oscillation show some discrepancies with investigations in other wave tanks (e.g. Shemer & Lichter 1987). This difference is probably due to non-ideal effects, such as viscous dissipation, capillary hysteresis, and turbulence at the wavemaker (Kit & Shemer 1989) which are geometry dependent.

The frequency-locked tongues from the sine map (figure 1) should be compared to the experimental tongues (figures 3 and 7). The width of the tongues increases with the non-linearity $K$ or the forcing amplitude $a^2$, and the winding number changes monotonically with frequency. Note that the observed tongues are locked to rational winding numbers with small denominators. Also, many of the tongues correspond to Farey daughters of the adjacent tongues; for example, $w(F_1/F_2) = \frac{2}{5}$ is the Farey daughter of $\frac{1}{2}$ and $\frac{1}{3}$ and $w(F_0/F_2) = \frac{25}{2}$ is the Farey daughter of $\frac{12}{1}$ and $\frac{13}{1}$. The winding number $w(F_1/F_2)$ $[w(F_0/F_2)]$ is graphed for a path through parameter space transverse to the tongue structure in figure 5 (figure 6). Note that the graph is a non-decreasing (non-increasing) function, with flat steps that can be identified with locked frequencies. This structure corresponds to the devil's staircase-type behaviour discussed in §2. Presumably, a finer examination would reveal a greater number of steps corresponding to locked intervals.

Inside the quasi-periodic tongues regions exist in which both winding numbers were rationally related and so all three frequencies were locked through weak coupling. It may be that the interaction of the three frequencies can be described by two weakly coupled circle maps (Coullet, Tresser & Arneodo 1980). However, these types of maps are still only partially understood (Linsay & Cumming 1989; Cumming & Linsay 1988).

At low forcing amplitudes (outside the subharmonic tongues), bands of chaos fell between the two-frequency quasi-periodic tongues, as suggested by Linsay & Cumming (1989) and Cumming & Linsay (1988) for the Newhouse–Ruelle–Takens scenario (Newhouse *et al.* 1978). Within the subharmonic tongues, a typical transition from periodic to chaotic behaviour can be seen in figures 8 and 9. There has already been one Hopf bifurcation to the sloshing modulation in figures 8(*b*) and 9(*b*), and the sloshing period is locked to the subharmonic. The states shown in figures 8(*c*, *d*) and 9(*c*, *d*) correspond to a second Hopf bifurcation. Presumably, the motion was near a three-torus when the one-mode became unlocked from the subharmonic and broke down into the chaotic state of figures 8(*e*) and 9(*e*).

By analogy to the circle map, the frequency-locked tongues should, at a critical

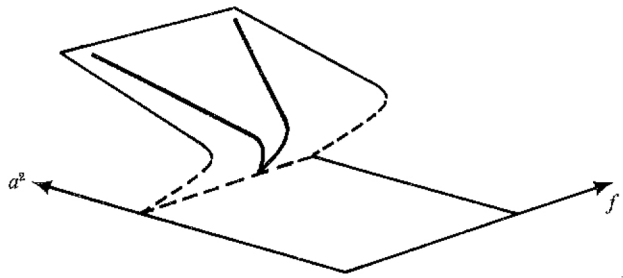


FIGURE 16. The quasi-periodic tongues shown in figures 3 and 7 do not reduce to a point as the forcing amplitude is decreased. One explanation is that the tongues are folded under the subcritical sloshing bifurcation as shown.

forcing amplitude, shrink to zero width. This was, in fact, seen in the subharmonic tongues. However, the quasi-periodic tongues, which are not locked to the driver, characteristically were of finite width along the transition line that delineates their initial appearance. This transition was hysteretic and can be interpreted as a subcritical bifurcation in which the tongues were tucked under (figure 16), onto the unstable branch (Anosov & Arnold 1988). The tips would then lie on the unstable branch, and only the truncated tongue would be observed.

The present observations also caution against relying exclusively on perturbation equations, such as the non-linear Schrödinger equation (NLS), in which the subharmonic frequency is averaged out. One can use NLS to describe the one-mode and sloshing modulations, as they occur on a long timescale. However, the NLS does not contain the fast timescale needed to describe the locking to the driving frequency.

Near the codimension two point, we found the stable mixed-mode state predicted by Ayanle *et al.* (1990). This state could only be reached by approaching it from the neighbourhood of the stable mode $N = 6$ fixed point. The stable mixed mode was composed of two modes ($N = 6, 7$) with a fixed phase relation. As the mode numbers differ by one, the modes were in phase on one side of the tank and out of phase on the other. On the in-phase side of the tank, the wave height was large; on the out-of-phase side, the wave height was small.

For sloshing to occur, the phase relation between the modes must change as a function of time (figure 12). This trajectory was taken in the $w(F_0/F_2) = 13$ subharmonic tongue, near the tip for which the one-mode oscillation is absent. The even modes $N$ were flipping between the two configurations $\cos(Ny)$ and $-\cos(Ny)$ that satisfy the boundary conditions on the sidewall of the tank (here, assumed to be at 0 and $2\pi$) as the odd modes oscillate about a non-zero mean. Before the one-mode oscillation appeared, the phase plane plot was approximately symmetric about a horizontal line. A small asymmetry was imposed by the odd number (13) of subharmonic cycles in one sloshing period. When the one-mode oscillation appeared, it broke the symmetry of the trajectory, yielding more complicated sloshing states. Typically, this symmetry breaking (figure 11) would lead to a pitchfork bifurcation (Guckenheimer & Holmes 1983). Note that the bifurcation is slightly imperfect; this may be related to the slight asymmetry of the sloshing before the one-mode oscillation is present. After the bifurcation, the system is in a periodic state where all three frequencies are present and locked.

Above the neutral stability curve NS+ for $f \lesssim 1.00$ for mode 7, two transversely propagating waves appeared and created irregular motion. This situation appears to

be similar to the irregular motion of the bidirectional azimuthal waves in the cylindrical geometry of parametrically forced waves in the experiments of Funakoshi & Inoue (1988).

At large cross-wave amplitudes, the noisy periodic states, consisting of two or more waves traversing the span of the tank, appeared. These waves became progressively more localized and appeared soliton-like as the forcing amplitude was increased. This may be related to the Benjamin–Feir instability of a uniform wavetrain and suggests that for an experimental apparatus capable of exciting high spanwise wavenumbers, solitons may dominate the dynamics.

The authors thank Charles Tresser for his interest in this problem during his stay at The University of Arizona. This work was encouraged through grants from the Office of Naval Research (N00014-86-K-0617, N00014-89-0-1748) and the National Science Foundation (MSM-8611379).

## REFERENCES

Anosov, D. V. & Arnold, V. I. 1988 Dynamical systems I. In *Ordinary Differential Equations and Smooth Dynamical Systems*. Springer.

Arneodo, A., Coullet, P. H. & Spiegel, E. A. 1983 Cascade of period doublings of tori. *Phys. Lett.* **94**A, 1–6.

Aronson, D. G., Chory, M. A., Hall, G. R. & McGehee, R. P. 1982 Bifurcations from an invariant circle for two-parameter families of maps of the plane: a computer-assisted study. *Commun. Math. Phys.* **83**, 303–354.

Ayanle, H., Bernoff, A. J. & Lichter, S. 1990 Spanwise modal competition in cross-waves. *Physica* D **43**, 87–104.

Bak, P., Bohr, T. & Jensen, M. H. 1985 Mode-locking and the transition to chaos in dissipative systems. *Phys. Scripta* T**9**, 50–58.

Barnard, B. J. S. & Pritchard, W. G. 1972 Cross-waves; part 2. Experiments. *J. Fluid Mech.* **55**, 245–255.

Chen, J. M. 1987 Subharmonic resonance of nonlinear cross-waves: theory and experiments. PhD thesis, The University of Arizona, Tucson.

Ciliberto, S. & Gollub, J. B. 1984 Pattern competition leads to chaos. *Phys. Rev. Lett.* **52**, 922–925.

Ciliberto, S. & Gollub, J. B. 1985 Chaotic mode competition in parametrically forced surface waves. *J. Fluid Mech.* **158**, 381–398.

Coullet, P., Tresser, C. & Arneodo, A. 1980 Transition to turbulence for doubly periodic flows. *Phys. Lett.* **77** A, 327–331.

Cumming, A. & Linsay, P. S. 1988 Quasiperiodicity and chaos in a system with three competing frequencies. *Phys. Rev. Lett.* **60**, 2719–2722.

Ecke, R. E., Farmer, J. D. & Umberger, D. K. 1989 Scaling of the Arnold tongues. *Nonlinearity* **2**, 175–196.

Funakoshi, M. & Inoue, S. 1987 Chaotic behaviour of resonantly forced surface water waves. *Phys. Lett.* A **121**, 229–232.

Funakoshi, M. & Inoue, S. 1988 Surface waves due to resonant horizontal oscillation. *J. Fluid Mech.* **192**, 219–247.

Grassberger, P. & Procaccia, I. 1983 Measuring the strangeness of strange attractors. *Physica* **9** D, 189–208.

Gu, X. M. & Sethna, P. R. 1987 Resonant surface waves and chaotic phenomena. *J. Fluid Mech.* **183**, 543–565.

Gu, X. M., Sethna, P. R. & Narain, A. 1988 On three-dimensional nonlinear subharmonic resonant surface waves in a fluid: part 1 – theory. *J. Appl. Mech.* **55**, 213–219.

Guckenheimer, J. & Holmes, P. 1983 *Nonlinear Oscillations, Dynamical Systems, and Bifurcations of Vector Fields*, Chapter 7. Springer.

Jones, A. J. 1984 The generation of cross-waves in a long deep channel by parametric resonance. *J. Fluid Mech.* **138**, 53–74.

Kit, E. & Shemer, L. 1989 On the neutral stability of cross-waves. *Phys. Fluids* **1**, 1128–1132.

Lichter, S. & Bernoff, A. J. 1988 Stability of steady cross-waves: theory and experiment. *Phys. Rev.* A **37**, 1663–1667.

Lichter, S. & Chen, J. 1987 Subharmonic resonance of nonlinear cross-waves. *J. Fluid Mech.* **183**, 451.

Lichter, S. & Underhill, W. B. 1987 Mode-number shifting of nonlinear cross-waves. *Phys. Rev.* A **35**, 5282–5284.

Linsay, P. S. & Cumming, A. 1989 Three-frequency quasiperiodicity, phase locking, and the onset of chaos. *Physica* D **40**, 196–217.

MacKay, R. S. & Tresser, C. 1986 Transition to topological chaos for circle maps. *Physica* **19** D, 206–237.

Miles, J. W. 1984 Nonlinear Faraday resonance. *J. Fluid Mech.* **146**, 285–302.

Newhouse, S., Ruelle, D. & Takens, F. 1978 Occurrence of strange axiom A attractors near quasperiodic flows on $T^m m \geqslant 3$. *Commun. Math. Phys.* **64**, 35–40.

Shemer, L. & Lichter, S. 1987 Identification of cross-wave regimes in the vicinity of a cut-off frequency. *Phys. Fluids* **30**, 3427–3433.

Shemer, L. & Lichter, S. 1990 The mode number dependence of neutral stability of cross-waves. *Exps Fluids* **9**, 148–152.

Simonelli, F. & Gollub, J. P. 1988 Stability boundaries and phase-space measurement for spatially extended dynamical systems. *Rev. Sci. Instrum.* **59**, 280–284.

Takens, F. 1981 Detecting strange attractors in turbulence. *Lecture Notes in Maths*, vol. 898, pp. 366–381.

Underhill, W. B. 1990 Transitions to chaotic cross-waves: An experimental investigation. PhD thesis, The University of Arizona, Tucson.

Van Atta, C. W. & Gharib, M. 1987 Ordered and chaotic vortex streets behind circular cylinders at low Reynolds numbers. *J. Fluid Mech.* **174**, 113–133.

Virnig, J. C., Berman, A. S. & Sethna, P. R. 1988 On three-dimensional nonlinear subharmonic resonant surface waves in a fluid: part II – experiment. *Trans. ASME* **55**, 220–224.

Wolf, A., Swift, J. B., Swinney, H. L. & Vastano, J. A. 1984 Determining Lyapunov exponents from a time series. *Physica* **16** D, 285–317.

Wu, J., Keolian, R. & Rudnick, I. 1984 Observation of a non-propagating hydrodynamic soliton. *Phys. Rev. Lett.* **52**, 1421–1424.